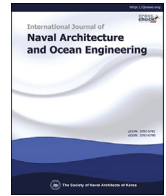


Contents lists available at [ScienceDirect](#)

International Journal of Naval Architecture and Ocean Engineering

journal homepage: <http://www.journals.elsevier.com/international-journal-of-naval-architecture-and-ocean-engineering/>

CFD validation and grid sensitivity studies of full scale ship self propulsion

Hrvoje Jasak ^{a, b}, Vuko Vukčević ^{a, *}, Inno Gatin ^a, Igor Lalović ^c

^a University of Zagreb, Faculty of Mechanical Engineering and Naval Architecture, Ivana Lučića 5, Zagreb, Croatia

^b Wikki Ltd, 459 Southbank House, SE1 7SJ, London, United Kingdom

^c Uljanik d.d., Flaciusova 1, Pula, Croatia

ARTICLE INFO

Article history:

Received 8 July 2017

Received in revised form

15 December 2017

Accepted 17 December 2017

Available online xxx

Keywords:

Full scale ship propulsion

Actuator disc

Sea trial validation

Grid sensitivity studies

OpenFOAM

ABSTRACT

A comparison between sea trial measurements and full-scale CFD results is presented for two self-propelled ships. Two ships considered in the present study are: a general cargo carrier at Froude number $F_n = 0.182$ and a car carrier at $F_n = 0.254$. For the general cargo carrier, the propeller rotation rate is fixed and the achieved speed and trim are compared to sea trials, while for the car carrier, the propeller rotation rate is adjusted to achieve the 80% MCR. In addition, three grids are used for each ship in order to assess the grid refinement sensitivity. All simulations are performed using the Naval Hydro pack based on foam-extend, a community driven fork of the OpenFOAM software. The results demonstrate the possibility of using high-fidelity numerical methods to directly calculate ship scale flow characteristics, including the effects of free surface, non-linearity, turbulence and the interaction between propeller, hull and the flow field.

© 2018 Society of Naval Architects of Korea. Production and hosting by Elsevier B.V. This is an open access article under the CC BY-NC-ND license (<http://creativecommons.org/licenses/by-nc-nd/4.0/>).

1. Introduction

Traditionally, features of engineering significance in marine hydrodynamic flows at full scale are deduced from extrapolation of the experimental model scale results. The practical limitations of matching both Reynolds and Froude scales simultaneously in towing tanks are well known. Additionally, extrapolating self-propulsion results from model scale to full scale is problematic due to inherently different flow conditions near the propeller. In contemporary engineering practice, these limitations are reliably circumvented by the vast practical experience and unique extrapolation procedures for standard hull forms (e.g. ITTC correlation lines). Recent regulations regarding Energy Efficiency Design Index (EEDI) (see e.g. R. MPEC.245(66), 2014) have increased the worldwide research in marine hydrodynamics, where Computational Fluid Dynamics (CFD) tools play an important role at predicting the flow field with Energy Saving Devices (ESDs). In their recent work, Visonneau et al. (2016) performed CFD simulations for the Japan

Bulk Carrier (JBC) (Larsson et al., 2015a, 2015b) and showed significant differences in flow field at the stern in model and full scale. Similar differences were observed by Castro et al. (2011) for a ship without an ESD. They performed CFD self-propulsion simulations in model and full scale, with discretised propeller and concluded that the propeller performance is more favourable in full scale because of the more uniform inflow to the propeller caused by a thinner boundary layer compared to model scale.

Predicting the self-propulsion point of the ship is one of the main practical problems in marine hydrodynamics. Due to high cost, uncertainty and severely limited availability of sea trial measurements, the CFD studies at model scale represent an active area of research (Carrica et al., 2010; Xing-Kaeding and Gatchell, 2015; Kim and Jun, 2015) as they provide an opportunity to validate the numerical methods against measured data. However, there seems to be an ongoing effort for directly comparing full scale CFD simulations with sea trials as discussed by Ponkratov and Zegos (2014, 2015). Comparing their full scale CFD results with sea trials, they obtained encouraging results for a medium range tanker. The increasing trend of performing full scale CFD simulations is witnessed by the recent Workshop on Ship Scale Hydrodynamic Computer Simulations (Lloyd's Register, 2016; Ponkratov, 2017), first of its kind, organized by the Lloyd's Register in 2016. The Workshop provides an unique opportunity for worldwide CFD

* Corresponding author.

E-mail addresses: hrvoje.jasak@fsb.hr, h.jasak@wikki.co.uk (H. Jasak), vuko.vukcevic@fsb.hr (V. Vukčević), inno.gatin@fsb.hr (I. Gatin), Igor.Lalovic@uljanik.hr (I. Lalović).

Peer review under responsibility of Society of Naval Architects of Korea.

<https://doi.org/10.1016/j.ijnaoe.2017.12.004>

2092-6782/© 2018 Society of Naval Architects of Korea. Production and hosting by Elsevier B.V. This is an open access article under the CC BY-NC-ND license (<http://creativecommons.org/licenses/by-nc-nd/4.0/>).

research community to directly compare their self-propulsion computations with sea trials via a blind test, followed by a public comparison of CFD results from various groups (Ponkratov, 2017).

The self-propulsion of a ship in CFD simulations requires adequate representation of the propeller. The hull-propeller interaction can be taken into account in a number of ways. The most efficient approach from the computational point of view is to model the propeller as an actuator disc; see Tzabiras et al. (2009) for successful application of the actuator disc. Another possibility is to use a fully discretised propeller, where the propeller rotation is enabled by either a sliding interface approach (Ponkratov and Zegos, 2015) or dynamic overset grids (Carrica et al., 2015; Shen et al., 2015). Although this approach is the most detailed approach without any modelling, it requires significant computational resources. The high demand on computational resources forced researchers to come up with different ways to speed their CFD computations without significantly sacrificing the accuracy. As an example, Ponkratov and Zegos (2015) use the Multiple Reference Frame (MRF) approach (also known as the "Frozen Rotor Approach") until the free surface converges and then start rotating the propeller. Recently, Carrica et al. (2015) introduced a partially rotating frame approach, which is a combination of the MRF approach and full propeller rotation. The approach allowed them to increase the time step by one order of magnitude; while still being able to capture a part of the hull-propeller interaction.

In this work, the primary goal is to validate the integral (global) characteristics of a self-propelled ship (eg achieved speed, propeller rotation rate, etc.) in a CPU time efficient manner, while the local flow features near the propeller are neglected. For this reason, the actuator disc model as described by Šeb (2017) is used to complement the two-phase, turbulent CFD model described below. In order to be able to assess the advance speed from the self-propulsion simulation with the actuator disc model, we perform an actuator disc analysis of the momentum transfer from the propeller to the fluid. The advance speed can then be readily used to calculate the pressure and tangential velocity jumps from the thrust and torque curves. Such a procedure allows one to run a single self-propulsion computation without the need to perform a special procedure as explained by Krasilnikov (2013), where two simulations have to be run side-by-side to establish the effective wake field at the propeller plane.

The CFD model is based on Reynolds Averaged Navier–Stokes equations for incompressible, free surface and transient flow field, with the $k - \omega$ SST (Menter et al., 2003) model to account for turbulence. The algebraic Volume-of-Fluid (VOF) method (Ubbink and Issa, 1999) is used to capture the free surface. The interface is kept sharp with the additional compressive term (Rusche, 2002), preventing the excessive smearing of the viscous stresses at the free surface. Although the smearing of viscous effects at the free surface is determined by the numerical smearing of the VOF field, the density and pressure gradient fields always have infinitesimally sharp distribution due to the Ghost Fluid Method (GFM) (Vukčević, 2016; Vukčević et al., 2017). The numerical model is implemented in the Naval Hydro pack and it is based on arbitrary polyhedral, cell-centred Finite Volume (FV) framework available within foam-extend-4.0, which is a community driven fork of the OpenFOAM software for Computational Continuum Mechanics (CCM) (Weller et al., 1998).

In this paper, two sets of full scale CFD self-propulsion computations are performed and results are compared to sea trial measurements for two types of ships. The first ship is the general cargo carrier REGAL with publicly available ship parameters and results from the sea trials, published during the Lloyd's Workshop

on Ship Scale Computer Simulation (Ponkratov, 2017). The sea trials have been performed by keeping the propeller rotation rate constant and measuring the achieved ship speed. This test is easily modelled with the actuator disc where the pressure jump and velocity swirl jump are evaluated based on thrust and torque obtained from the corrected advance coefficient during the CFD computation. The second ship is a car carrier built in the Croatian shipyard Uljanik, where only limited data can be provided due to confidentiality agreement. The CFD computations for the car carrier correspond to the measured mile sea trial, where the 80% Maximum Continuous Rating (MCR) is prescribed and the achieved speed and propeller rotation rate is measured. The Proportional–Integral (PI) controller is used to effectively reach the prescribed power with varying propeller rotation rate. Computations for both ships are performed on three unstructured grids each, in order to estimate the sensitivity of the solution with respect to grid refinement.

The paper is organized in the following manner. The mathematical and numerical models are presented first, with emphasis on the actuator disc model and the procedure for calculating the advance speed from the sampled axial speed at the propeller plane. The computational results for the REGAL ship are presented next, including: the details regarding computational grids, open water simulation results, comparison of achieved speed and trim with sea trial measurements and simplified uncertainty assessment. The Uljanik car carrier is considered next, where the achieved power, propeller rotation rate and ship speed are compared to measured mile data, including the grid uncertainty assessment. A short conclusion is given at the end, reflecting on achieved results and discussing the practicality and accuracy of full scale self-propulsion simulations.

2. Mathematical and numerical modelling

The final form of governing equations for a two-phase, incompressible, turbulent flow is presented here, while the reader is referred to Vukčević et al. (2017) and Vukčević (2016) for a detailed derivation. The free surface discontinuities are handled with the GFM (Huang et al., 2007; Desjardins et al., 2008; Lalanne et al., 2015), while the interface is captured using the VOF approach (Aulisa et al., 2003; Røenby et al., 2016) in an implicit, algebraic formulation (Ubbink and Issa, 1999; Rusche, 2002). Turbulence is modelled with the $k - \omega$ SST turbulence model (Menter et al., 2003) with standard wall functions. The actuator disc model (Šeb, 2017) is presented and the special attention is given to the calculation of advance speed during the CFD simulation.

2.1. Governing equations

The presence of a free surface in the domain of interest Ω , requires certain jump conditions to be taken into account. The jump conditions are denoted with $[\cdot]$ as used by e.g. Huang et al. (2007) and are outlined here:

- Density discontinuity:

$$[\rho] = \rho_a - \rho_w, \quad \mathbf{x} \in \Gamma, \quad (1)$$

where ρ_a is water density and ρ_w is air density, and Γ denotes the free surface. Note that the density jump conditions simply indicates that the density field ρ is a piece-wise constant function of space and time.

- Continuity of pressure p :

$$[p] = 0, \quad \mathbf{x} \in \Gamma. \quad (2)$$

Note that the surface tension effects are neglected.

- An additional jump condition for pressure gradient can be derived by taking into account continuity of velocity field at the free surface (kinematic boundary condition [Batchelor, 1967](#)) and neglecting the tangential stress balance at the free surface ([Vukčević, 2016](#)):

$$\left[\frac{\nabla p}{\rho} \right] = 0, \quad \mathbf{x} \in \Gamma, \quad (3)$$

indicating that the pressure gradient divided by the density does not have a discontinuity at the free surface. This can be easily understood when examining the hydrostatic case ([Queutey and Visonneau, 2007](#)), while it is important to note that this assumption is valid even in non-hydrostatic cases ([Vukčević, 2016](#)).

- It is important to note that other fields are continuous at the free surface. Velocity field \mathbf{u} is continuous across the free surface due to kinematic boundary condition (see [Batchelor, 1967](#)), while the specific turbulent kinetic energy k and specific dissipation rate of the turbulent kinetic energy ω are also continuous ([Huang et al., 2007](#)) since they depend only on the velocity field \mathbf{u} .

It is important to clearly state the assumptions and simplifications within the present model:

- The tangential stress balance at the free surface is simplified by assuming a continuous effective kinematic viscosity across the free surface. Although continuous, the effective kinematic viscosity has a large gradient near the free surface as defined by the volume fraction field (see Eq. (8) for details). [Huang et al. \(2007\)](#) showed that this approach is valid for large Reynolds numbers encountered in ship hydrodynamic flows, which are considered in this work.
- The surface tension effects can also be neglected for full scale ship hydrodynamics flows. The reader is referred to [Vukčević \(2016\)](#) for additional details.

If the jump conditions given by Eqs. (1)–(3) are taken into account, the flow field in both phases can be described with the continuity equation and Navier-Stokes equations in terms of primitive variables: velocity field \mathbf{u} and dynamic pressure field p_d , and the spatial variation of density can be neglected, as it is only present in a form of the Heaviside function at the interface:

$$\nabla \cdot \mathbf{u} = 0, \quad \mathbf{x} \in \Omega, \quad (4)$$

$$\frac{\partial \mathbf{u}}{\partial t} + \nabla \cdot (\mathbf{u}\mathbf{u}) - \nabla \cdot (\nu_e \nabla \mathbf{u}) = -\frac{\nabla p_d}{\rho}, \quad \mathbf{x} \in \Omega, \quad (5)$$

where ν_e is the effective viscosity field with a smeared profile across the free surface, and p_d is the dynamic pressure defined as:

$$p_d = p - \rho \mathbf{g} \cdot \mathbf{x}, \quad (6)$$

where \mathbf{x} is the position vector. The VOF method is used to capture the interface:

$$\frac{\partial \alpha}{\partial t} + \nabla \cdot (\mathbf{u}\alpha) + \nabla \cdot (\mathbf{u}_r \alpha (1 - \alpha)) = 0, \quad (7)$$

where α is the volume fraction and \mathbf{u}_r is the compressive velocity field acting in the normal direction towards the interface, explained in detail in Sec. 2.3. The third term in Eq. (7) is introduced to keep the interface from excessive smearing ([Rusche, 2002](#)). The term is active only near the free surface due to $\alpha(1 - \alpha)$ prefactor that vanishes for $\alpha = 0, 1$. Note that the smearing of the interface only affects the viscous stresses at the free surface since we define the effective kinematic viscosity field as:

$$\nu_e = \alpha \nu_{e,w} + (1 - \alpha) \nu_{e,a}. \quad (8)$$

Note that the smearing of α does not affect the density field, since we define:

$$\rho(\mathbf{x}) = \begin{cases} \rho_w, & \text{if } \alpha(\mathbf{x}) \geq 0.5, \\ \rho_a, & \text{if } \alpha(\mathbf{x}) < 0.5. \end{cases} \quad (9)$$

The piece-wise constant definition of the density field given by Eq. (9) is taken into account with the GFM, which is practically embedding the discontinuities at the free surface during the discretisation process. Note that with this definition, we achieve an infinitesimally sharp jump of density and pressure gradient at $\alpha = 0.5$ iso-surface.

2.2. Actuator disc model

The outline of the actuator disc model used in this work is given here, while the reader is referred to [Šeb \(2017\)](#) for detailed derivation and validation. The actuator disc is a circular surface defined by three parameters:

1. Location of the propeller plane,
2. Direction of the propeller action,
3. Propeller radius.

Such definition makes it suitable for CFD calculations in FV framework, where a set of faces can be readily collected from the computational grid.

The pressure jump at the actuator disc is modelled as:

$$\Delta p = \frac{105}{8} \frac{T(J)}{\pi(R_p - R_H)(3R_H + 4R_p)} f_T(r) \quad (10)$$

where R_p is the propeller radius, R_H is the hub radius, $T(J)$ is the propeller thrust for a given advance coefficient J and $f_T(r)$ is defined as:

$$f_T(r) = r^* \sqrt{1 - r^*}. \quad (11)$$

r^* is the normalised disc radius defined as:

$$r^* = \frac{r' - r'_h}{1 - r'_h}. \quad (12)$$

while $r' = r/R_p$ and $r'_h = R_H/R_p$. The tangential velocity jump models the swirl caused by the propeller action and is given by:

$$\Delta u_t = \frac{105}{8} \frac{Q(J)}{\rho \pi u_x (R_p - R_H)(3R_H + 4R_p)} f_Q(r). \quad (13)$$

where $Q(J)$ is the propeller torque for a given advance coefficient, u_x is the axial speed at the propeller plane and $f_Q(r)$ is given by:

$$f_Q(r) = \frac{r^* \sqrt{1-r^*}}{r^*(1-r^*) + r_h'} \quad (14)$$

Eqs. (10) and (13) require thrust and torque curves from the open water test to determine the pressure and tangential velocity jump for the actuator disc model. The thrust and torque curves are usually given in dimensionless form with respect to the advance coefficient J , defined as:

$$J = \frac{V_A}{nD}, \quad (15)$$

where V_A is the advance speed (equal to carriage speed in experimental set-up for the open water test), n is the propeller rotation rate and D is the propeller diameter. In order to determine the advance speed from the self-propulsion CFD simulation, we note that the propeller in the actuator disc theory accelerates the flow from $V_1 = V_A$ in front of the propeller to V_2 behind the propeller. Therefore, the propeller thrust is proportional to the mass flux at the propeller plane and the difference in flow velocities:

$$T = \rho_w A_D V_D (V_2 - V_1), \quad (16)$$

where A_D is the actuator disc surface and V_D is the average axial speed at the propeller plane. With $V_D = 0.5(V_1 + V_2)$, we obtain an expression for the advance speed:

$$V_1 = V_A = V_D - \frac{T}{2\rho_w A_D V_D}. \quad (17)$$

Note that V_D can be readily evaluated from the CFD computation. However, although (17) provides an expression for the advance speed, it depends on the thrust, creating a nonlinear system of equations since T is a function of J . In practice, since the update of V_A given by (17), followed by the Δp update given by (10) happens several times during a single time-step in a segregated solution algorithm for pressure-velocity coupling, the nonlinear system is easily converged without employing an additional iterative loop.

2.3. Numerical model

Governing Eqs. (4), (5) and (7) are discretised using the second order accurate in space and time, arbitrary polyhedral FV method (Jasak, 1996) with compact computational support stencil. Time derivative terms are discretised with first-order accurate implicit Euler scheme since a quasi steady-state solution is sought. The convection term in the momentum equation is discretised using the Gauss theorem, where the linear, upwind-biased interpolation is used to interpolate from cell-centres to face-centres. The convection term in the VOF equation is discretised with van Leer's Total Variation Diminishing (TVD) scheme (van Leer, 1977) in a deferred correction approach (Ferziger and Peric, 1996). All diffusion terms are discretised using the Gauss theorem and central-differencing, with over-relaxed approach for the non-orthogonal correction (Jasak, 1996) (see Demirdžić, 2015 for different treatments for the non-orthogonal correction). For full details of the discretisation the reader is referred to Jasak (1996).

The compressive term in the VOF transport Eq. (7) is discretised using Gauss theorem:

$$\int_{V_p} \nabla \cdot (\mathbf{u}_r \alpha (1 - \alpha)) \approx \sum_f \mathbf{s}_f \cdot \mathbf{u}_r (1 - \alpha_f^o) \alpha_f^n = \sum_f F_{ar} \alpha_f^n, \quad (18)$$

where V_p is the volume of cell P , \sum_f denotes the sum over all faces

of a cell, \mathbf{s}_f is the surface area vector of a face directed towards the neighbouring cell. Superscripts o and n denote values from previous and current time step, respectively. Rusche (2002) defines the compressive velocity field \mathbf{u}_r as flow dependent, ie based on the flux through the free surface. A different approach is employed here, where the compressive velocity is defined as a purely numerical parameter:

$$\mathbf{u}_r = c_\alpha \mathbf{n}_\Gamma \frac{CFL_{ref} |\mathbf{d}_f|}{\Delta t}, \quad (19)$$

where c_α is the compression constant which controls the sharpness of the interface, usually taken as one. \mathbf{n}_Γ is the unit normal vector to the free surface, $CFL_{ref} = 0.5$ is the reference compression Courant-Friedrichs-Lewy number, Δt is the time step and $|\mathbf{d}_f|$ is the distance between cell centres sharing this internal face. Compared to Rusche (2002), the formulation for the compressive velocity field \mathbf{u}_r , used in this work given by (19) does not depend on the physical flux through the interface, making the compression purely a numerical parameter, which can be tuned to obtain desired sharpness of the interface. Interpolation of α_f from cell centres to face centre reads:

$$\alpha_f = w_f \alpha_P + (1 - w_f) \alpha_N, \quad (20)$$

where the weighting function w_f is defined in terms of limiter function ψ_f , central differencing weights w_{CD} and upwind weights w_U , following Jasak et al. (1999):

$$w_f = \psi_f w_{CD} + (1 - \psi_f) w_U. \quad (21)$$

A limiter based on quartic function is used in this work:

$$\psi_f = 1 - \max\left((1 - 4\alpha_P(1 - \alpha_P))^2, (1 - 4\alpha_N(1 - \alpha_N))^2\right), \quad (22)$$

as presented in Fig. 1. Looking at (21), the limiter is designed to be upwind biased if the interface is sharp (eg $\alpha_N \approx 0$ and $\alpha_P \approx 1$), while going toward central differencing if the interface is excessively smeared (eg $\alpha_N \approx \alpha_P \approx 0.5$). Note that the combination of van Leer's TVD limiter for the convection term and the quartic limiter for the

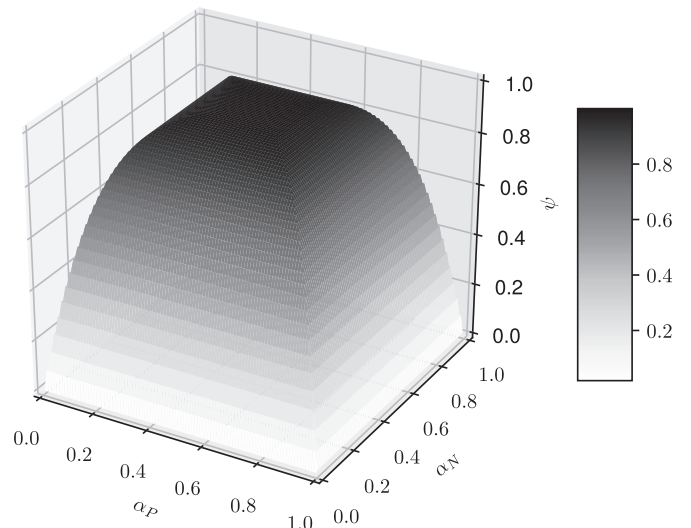


Fig. 1. Limiter function based on cell centred α values.

additional compressive term in general ensures boundedness of α . In practice, small unboundedness up to $1e-3$ does occur locally. However, this does not affect the stability and accuracy of the simulation since the GFM does not require density to be defined in terms of volume fraction. For details, the reader is referred to Vukčević et al.

The jump conditions at the free surface given by (1)–(3) are enforced during the discretisation process using the GFM (Vukčević et al., 2017), yielding interface-corrected interpolation schemes for fields with discontinuities: density and pressure.

The pressure–velocity coupling is resolved with a combination of SIMPLE (Patankar and Spalding, 1972) and PISO (Issa, 1986) algorithm, allowing the algorithm to advance with large time-steps and avoid the under-relaxation of governing equations and fields. Evolution of the free-surface and rigid body motion of a ship is embedded within the outer iteration loop. Two outer iterations are used along six PISO pressure correction steps in a given time step, updating the free surface and position of the ship two times, while correcting pressure and velocity twelve times in total. For details of the solution algorithm and rigid body motion treatment, the reader is referred to Vukčević et al. (2017).

Implicit relaxation zones are used to prevent wave reflection (Jasak et al., 2015), where the waves are gradually damped near the farfield boundaries using the exponential blending function (Jacobsen et al., 2012). Length of the relaxation zones are: $0.75L_{pp}$ for inlet, portside and starboard boundaries and $1.5L_{pp}$ for the outlet boundary.

The numerical algorithm is implemented in the Naval Hydro pack based on foam-extend-4.0, a scientific community driven fork of the open source software for applied continuum mechanics OpenFOAM (Weller et al., 1998).

3. Ship scale self-propulsion simulations

The CFD simulation results for two ships are presented in this section and directly compared to sea trial measurements. The first ship is the general cargo carrier REGAL from the Lloyd's Workshop on Ship Scale Hydrodynamic Computer Simulations (Lloyd's Register, 2016; Ponkratov, 2017) with fixed propeller rotation rate. The second ship is a car carrier from Uljanik shipyard where the 80% Maximum Continuous Rating (MCR) was fixed during the sea trial and the propeller rotation rate is reported. In addition, a basic grid uncertainty assessment is presented for both ships.

3.1. General cargo carrier REGAL

The main particulars of the REGAL ship are given in Table 1.

Table 1
Particulars of the REGAL general cargo carrier and sea trial conditions (Ponkratov, 2017).

Length between perpendiculars	L_{pp} , m	138
Breadth moulded	B , m	23
Depth moulded	D , m	12.1
Propeller diameter	D_p , m	5.2 (four bladed)
Service speed at design draught	V , kn	14
Water density	ρ_w , kg/m ³	1010
Kinematic viscosity of water	ν_w , m ² /s	8.8394×10^{-7}
Air density	ρ_a , kg/m ³	1.1649
Kinematic viscosity of air	ν_a , m ² /s	1.6036×10^{-5}
Longitudinal centre of gravity	LCG , m	71.266 (from A.P.)
Vertical centre of gravity	VCG , m	0.0 (free surface)
Transverse centre of gravity	TCG , m	-0.058 (starboard)
Mass	Δ , t	12881.27
Pitch radius of gyration	R_{yy} , m	$0.25L_{pp}$

Before the sea trials, the ship has been dry-docked, her hull cleaned and propeller polished. Within the Lloyd's Workshop On Ship Scale Computer Simulation (Ponkratov, 2017), surface meshes have been obtained with 3D laser scanning procedure and were provided to interested participants. The ship was taken to sea trials in ballast condition and three shaft speeds have been tested. In this work, we present a set of results obtained with three grids for a single shaft speed of 106.4 RPM, corresponding to a ship speed closest to the design speed.

3.1.1. Computational grids

Computational grids are generated with cfMesh (Juretić, 2017), an open-source mesher available within foam-extend. The computational domain is one L_{pp} in front of the ship, two L_{pp} behind the ship and one L_{pp} towards the starboard and portside and towards the bottom. Note that the symmetry plane is not used because the ship is fixed at a small roll angle (see Ponkratov, 2017 for details) and to allow for velocity swirl within the actuator disc model. In the present work, the superstructure and cranes on the deck were neglected in order to use coarser grids without significantly affecting the results.

Fig. 2(a) presents local surface refinements at the stern, clearly showing the actuator disc interface. Bow stem refinement is shown in Fig. 2(b), while Fig. 2(c) shows the Kelvin angle refinement. Aggressive refinement towards the free surface is used, which can be seen in Fig. 2(d).

Three grids with non-uniform refinement are generated for this test case, as follows: the coarse grid with 5.6 million cells, the medium grid with 7.5 million cells and the fine grid with 11.7 million cells. The refinement ratio based on average cell size is not uniform between the refinement levels: the refinement ratio between the medium and the fine grid is $r_{mf} = 1.2$, while the refinement ratio between the coarse and the medium grid is $r_{cm} = 1.1$. Results obtained with such a low refinement ratio cannot be reliably used to estimate achieved order of convergence and uncertainty. Rather, we use simplified methods reported by other authors (Stern et al., 2001; Simonsen et al., 2013) to determine uncertainty intervals based on three results, as reported in Sec. 3.1.3. Grids coarser than 5.6 million cells generated with cfMesh were unable to produce physically meaningful results due to too low resolution in the vertical direction near the free surface. The grids mostly have hexahedral cells (95%), with occasional general polyhedral cells (5%). Maximum non-orthogonality for the fine grid is approximately 88° , while the average value is approximately 7° . Six boundary layers are used with a growth ratio of 1.3, yielding an average dimensionless distance to the wall y^+ between 900 and 1100 across the three grids for the achieved speed.

3.1.2. Open water propeller simulations

As discussed in Sec. 2.2, thrust and torque curves from open water tests are needed to perform self-propulsion simulations with the actuator disc model. Since experimental open water data is not provided within the Lloyd's Workshop On Ship Scale Computer Simulation (Ponkratov, 2017), full scale open water simulations are performed using the Generalised Grid Interface (GGI) (Beaudoin and Jasak, 2008) to couple non-conformal grids at the rotating interface. The Multiple Reference Frame (MRF) approach is used to reach a steady state solution for a rotating propeller. Five simulations for advance ratios: 0.2, 0.3, 0.4, 0.5 and 0.6 are performed, while the advance ratio is varied by changing the advance speed V_A and keeping the propeller rotation rate fixed to $n = 71.62$ rpm. The open water results are presented in Fig. 3(a) in a dimensionless form, where $K_T = T/(\rho n^2 D_p^4)$ is the thrust coefficient, $K_Q = Q/(\rho n^2 D_p^5)$ is the torque coefficient, while $\eta_o = JK_T/(2\pi K_Q)$

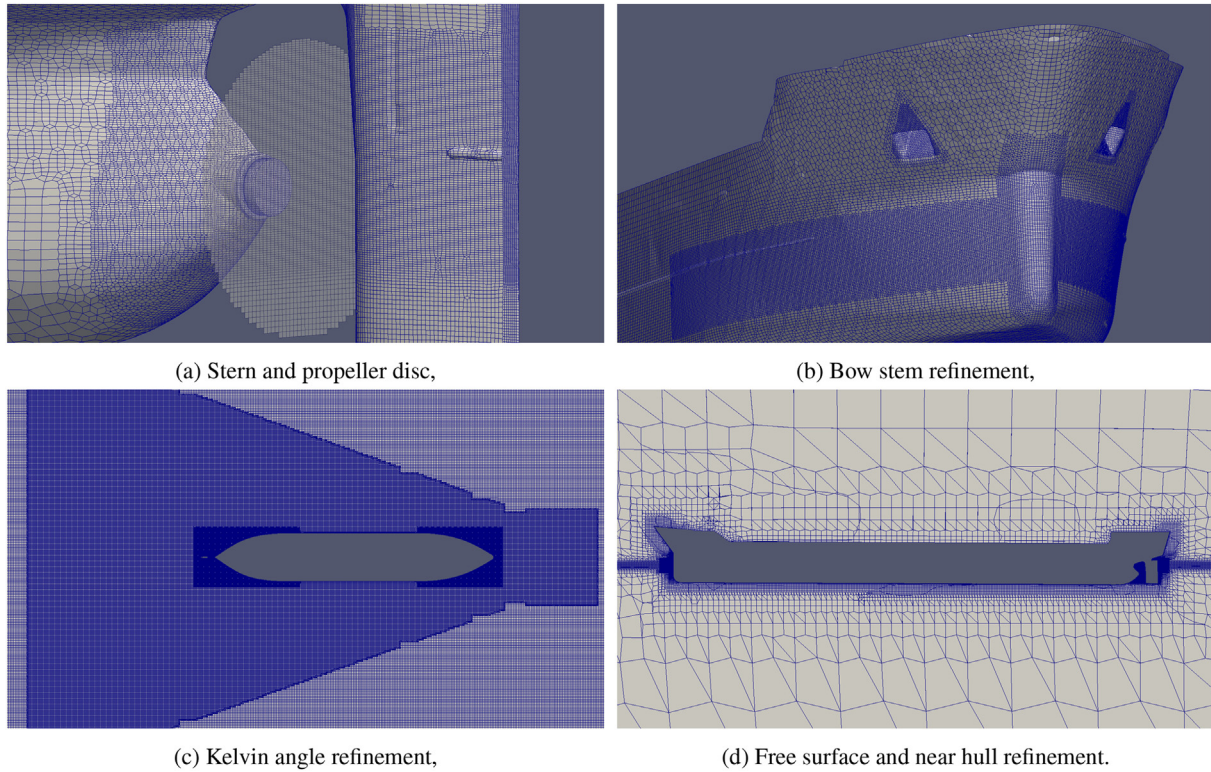


Fig. 2. Details of the fine grid.

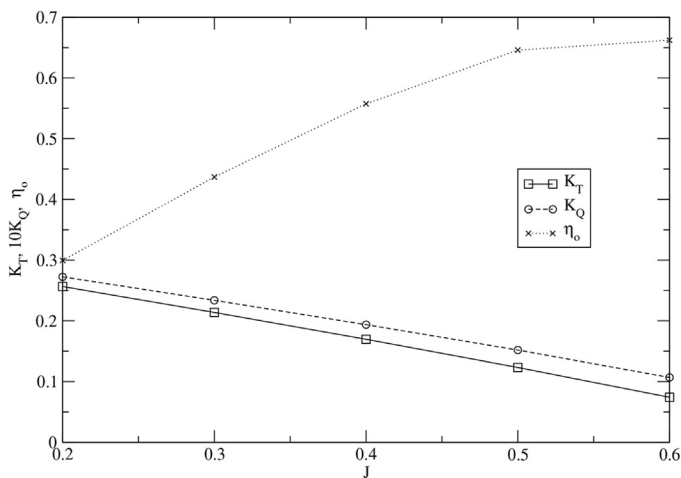
stands for open water efficiency. The vorticity field generated by the propeller in open water is shown in Fig. 3(b), where tip and hub vortices can be seen. No attempt has been made here to quantify the uncertainty with respect to grid refinement and solution settings, while the reader is referred to Šeb (2017) for additional details on our guidelines regarding open water propeller simulations.

3.1.3. Self-propulsion simulation results for REGAL ship

In self-propulsion simulations reported in this study, the ship is free to surge, heave and pitch, while sway, roll and yaw are constrained. A fixed time step $\Delta t = 0.075$ s is used, yielding maximum Courant–Friedrichs–Lewy (CFL) number of $\mathcal{O}(10^2)$, while the

mean CFL number is $\mathcal{O}(10^{-1})$.

The converged solution in terms of achieved forward speed of the ship is reached after 750 s for all three grids, which is equivalent to 10 000 time steps. The convergence of the forward speed for all three grids is presented in Fig. 4(a), where the results are compared with two sea trial measurements and the ISO 15016 value. All CFD results lie between the two sea trial measurements, with the relative error of CFD to the ISO 15016 is 0.2%. Following classification of grid convergence/divergence types as outlined by Eça and Hoekstra (Eça and Hoekstra, 2014), we achieve oscillatory converge with grid refinement. Stern et al. (2001) propose to use the following expression to evaluate the grid uncertainty in case of



(a) Open water CFD results,

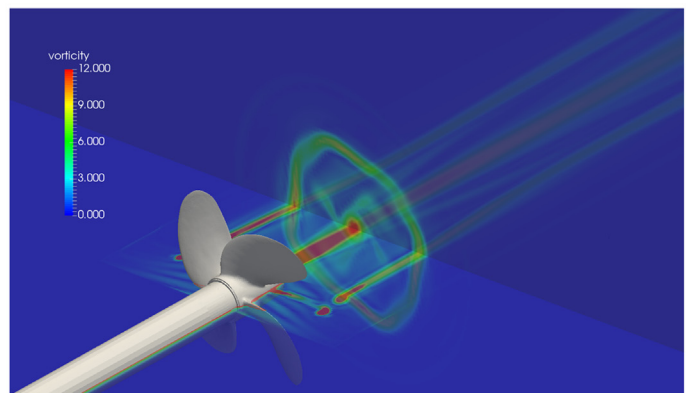
(b) Vorticity field ($\omega = \nabla \times \mathbf{u}$) generated by the propeller.

Fig. 3. CFD results for the open water test.

oscillatory convergence:

$$U_V = 0.5F_S(V_{\max} - V_{\min}), \quad (23)$$

where $F_S = 3$ is the safety factor and V_{\max} and V_{\min} in this case denote the maximum and minimum speeds obtained with three grids. Using the results presented in Fig. 4(a), the numerical uncertainty is approximately 0.02 knots, or 0.15% of the fine grid result. In addition to the forward speed results, convergence of dynamic trim is presented in Fig. 4(b), comparing the CFD results with sea trial measurements. The calculated values on all three grids under-predict the measured trim by 0.02° compared to the first sea trial and 0.028° compared to the second sea trial. Iterative uncertainty for the dynamic trim calculated with (23) yields an uncertainty of 0.025° for the coarse grid and 0.0028° for the fine grid, indicating that the convergence is smoother on finer grids.

Convergence of the absolute value of resistance and propeller thrust is presented in Fig. 5(a). Since a uniform flow field is used as an initial condition, the propeller thrust is smaller than the resistance of the ship up to approximately 150 s, causing the ship to decelerate (see Fig. 4a). After 150 s, the net thrust is positive, accelerating the ship forward. Finally, at approximately 600 s, the propeller thrust and resistance start to oscillate with ± 8 kN, or $\pm 2.5\%$ compared to the final solution taken as the average over past two hundred iterations. The viscous force oscillates with the amplitude of $\pm 0.15\%$, which is an order of magnitude smaller than the total force. In addition, the viscous force at achieved forward speed is compared with the ITTC 1957 correlation line, yielding a discrepancy of 2%.

The convergence of forces is significantly less oscillatory on medium and fine grids compared to the coarse grid, as indicated in Fig. 5(b). It is possible that the reason for inferior convergence on the coarse grid is directly linked to insufficient grid resolution near the free surface. However, after 600 s, all results oscillate by the same amount, indicating that the final result is insensitive to grid refinement. In the simulations, authors have noticed the occurrence of breaking waves in front of the bow due to vertical, cylindrical bow stem without a bulb, as indicated in Fig. 6(a). Similar flow features have been observed at the stern near the intersection of the rudder with a free surface, as seen in Fig. 6(b). In the accompanying video showing ten seconds of free surface flow near the bow, one can observe flow patterns with large periods of three to five seconds. Performing a Discrete Fourier Transform (DFT) for

resistance in last one hundred seconds reveals a spectrum with periods ranging from three seconds to seven seconds, as seen in Fig. 7. The video reveals numerically under-resolved wave breaking, which leads us to conclusion that finer grids should definitely be used in order to investigate this phenomena thoroughly, which is out of scope of this work.

Supplementary video related to this article can be found at <https://doi.org/10.1016/j.ijnaoe.2017.12.004>.

In order to discuss the practical engineering feasibility of these computations, CPU times for all simulations are presented in Table 2. Each simulation is carried out in parallel using up to 7 nodes (56 cores) on a distributed memory computational cluster: CPU—2x Intel Xeon E5-2637 v3 4-core, 3.5 GHz, 15 MB L3 Cache, DDR4—2133, with InfiniBand communication. It takes 39.4 h (1.6 days) to achieve convergence with the coarse grid and 83.8 h (3.5 days) with the fine grid. Note that one second of real time for such a full scale simulation requires $\mathcal{O}(10^2)$ seconds of CPU time using these particular computational resources. The actuator disc model allows a larger time-step to be used. If the discretised, rotating propeller is used, the time-step would be approximately $\mathcal{O}(10^2)$ times lower in order to resolve propeller motion with 0.5° per time step (eg as used by Shen et al., 2015).

3.2. Car carrier from Uljanik shipyard

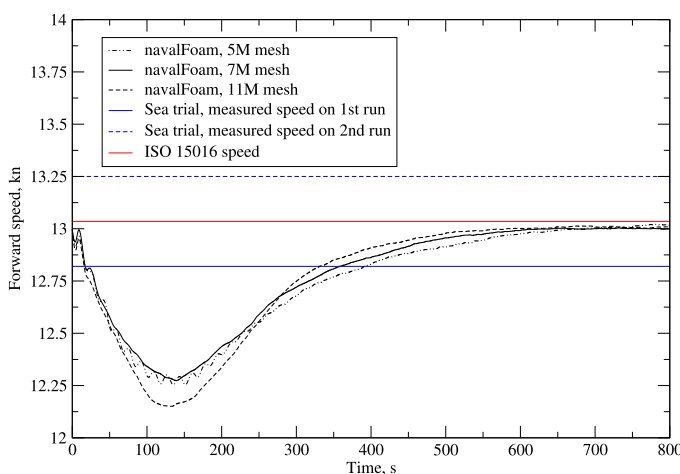
The second ship considered in this study is the car carrier built in Uljanik shipyard, with particulars given in Table 3. The input parameters for this test case were provided by Uljanik shipyard:

- Hull geometry,
- Propeller characteristics obtained from open water test in model scale,
- Target 80% MCR.

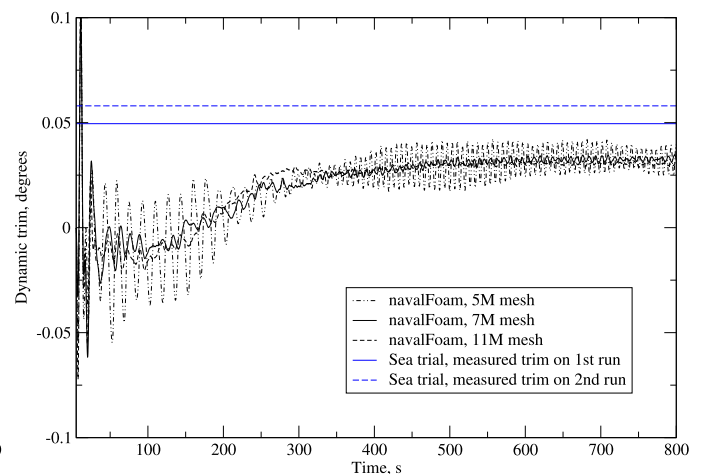
Since the target 80% MCR is given, a similar PI controller as used by Carrica et al. (2011) is employed in this study, defined as:

$$n = n' + K_P(P - P_{\text{target}}) + K_I \int_0^t (P - P_{\text{target}}) dt, \quad (24)$$

where n is the propeller revolution rate in RPS, n' is the propeller



(a) Convergence of forward speed,



(b) Convergence of dynamic trim,

Fig. 4. CFD results compared to sea trials.

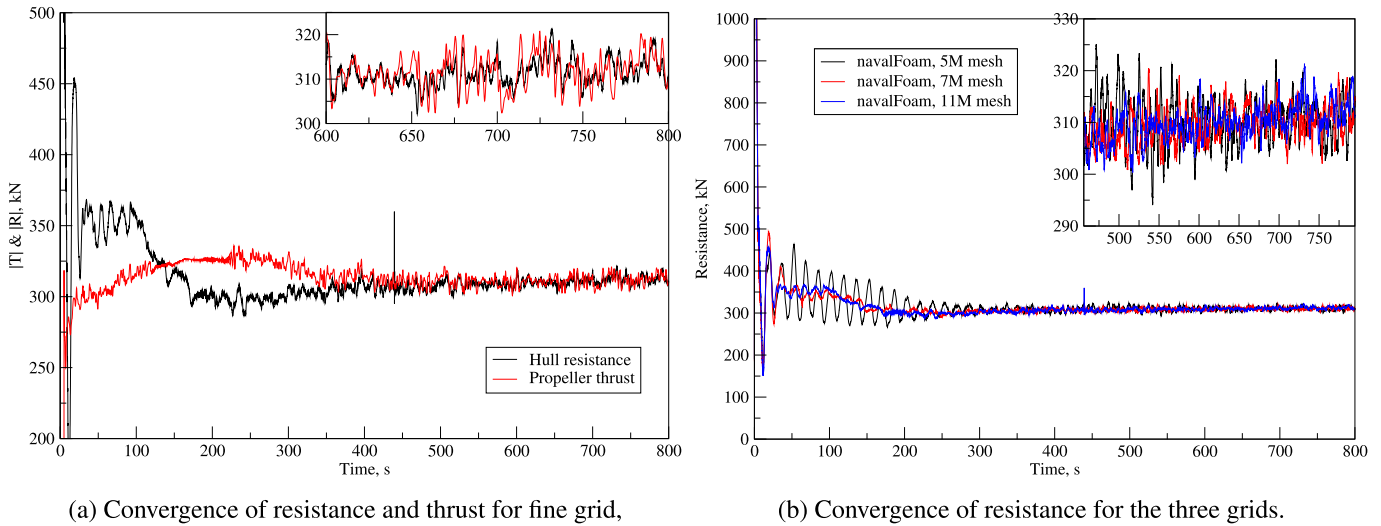


Fig. 5. Convergence of forces in CFD simulations.

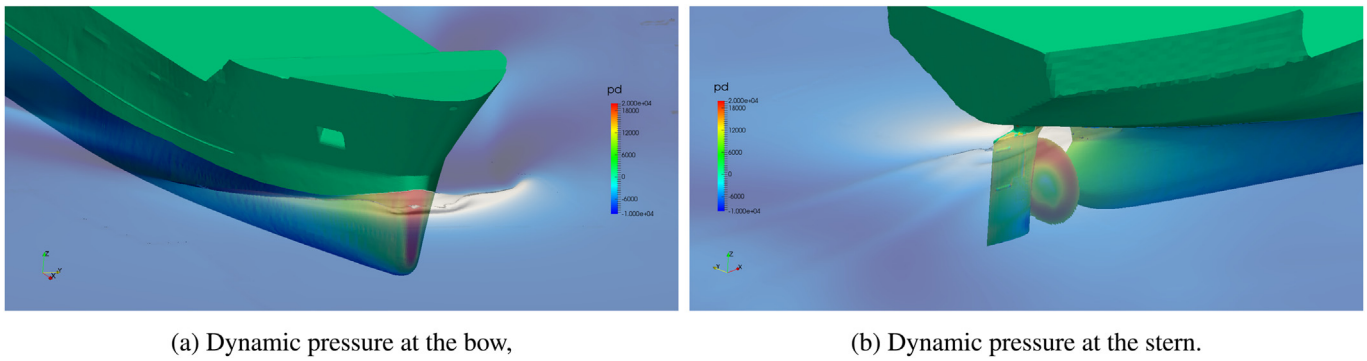


Fig. 6. Dynamic pressure field in bow and stern regions for REGAL ship.

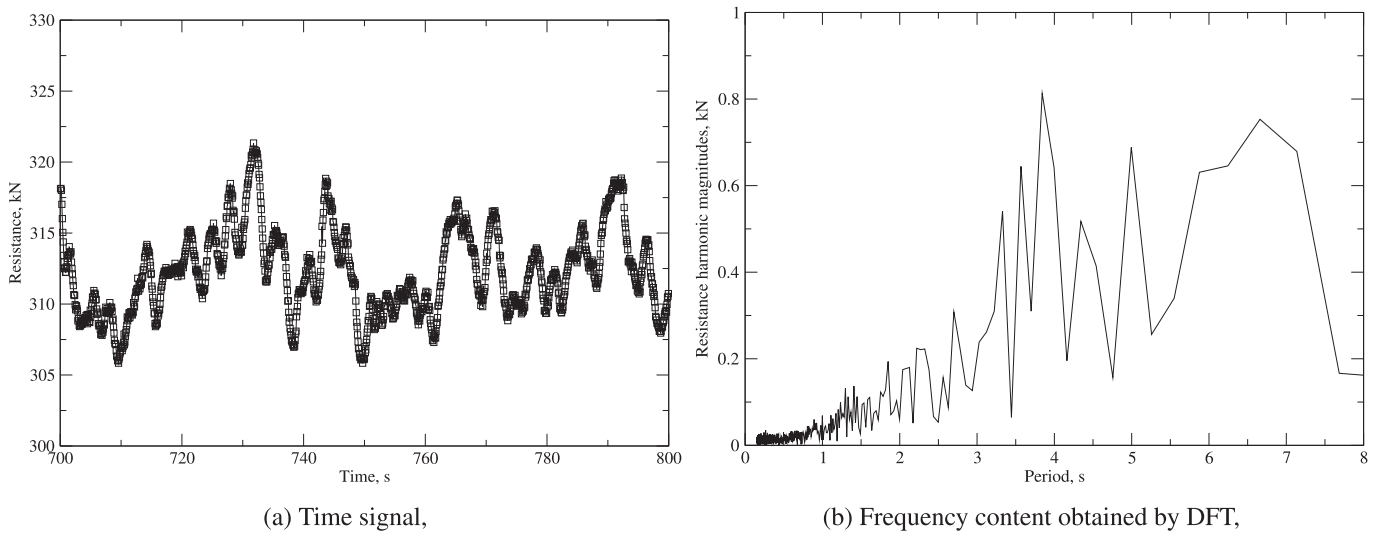


Fig. 7. Resistance for fine grid during last one hundred seconds.

revolution rate from the previous iteration, P is the current power and P_{target} is the target power. Proportional and integral constants are taken as $K_p = K_i = 1.0 \cdot 10^{-10}$. Using (24), propeller revolution rate

n is updated based on current achieved power P , providing new thrust and torque estimates for the actuator disc model (see Sec. 2.2).

Table 2

CPU times for general cargo carrier self-propulsion simulations.

Grid	Coarse	Medium	Fine
Number of cells	5 597 931	7469 642	11 727 781
Number of cores	48	48	56
CPU time per time-step, s	14.2	19.1	29.8
CPU time per second of real time	189.8	254.5	397.2
CPU time until convergence ($t = 750$ s), h	39.4	53.1	83.8

Table 3

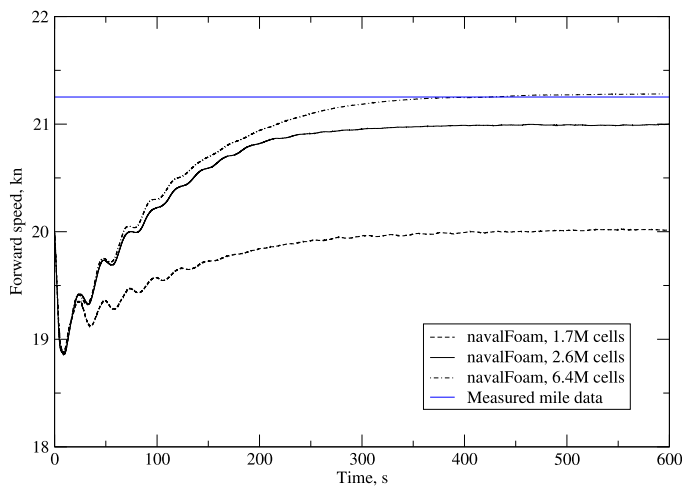
Particulars of the car carrier built in Uljanik shipyard.

Length between perpendiculars	L_{pp} , m	188.7
Breadth	B , m	32.26
Draft at sea trial	T , m	6.235
Propeller diameter	D_p , m	5.9 (four bladed)
Longitudinal centre of gravity	LCG , m	90.49 (from A.P.)
Vertical centre of gravity	VCG , m	0 (free surface)
Transverse centre of gravity	$TCCG$, m	0 (starboard)
Mass	Δ , t	20846.9
Power	80% MCR, kW	11376

Three unstructured grids are generated with cfMesh. The grids have 1.7, 2.6 and 6.4 million cells and consist of mostly hexahedral cells (approximately 95%) with occasional arbitrary polyhedral cells (5%). Maximum non-orthogonality for the fine grid is 72° , while the average non-orthogonality is 7° . Dimensionless wall distance y^+ is 4 580, 4520 and 4470 on coarse, medium and fine grid, respectively.

3.2.1. Self-propulsion simulation results for the Uljanik car carrier

Convergence history of the forward speed for three grids is presented in Fig. 8(a). Compared to REGAL ship, the car carrier immediately starts to accelerate since the initial speed is 5%–10% smaller than the measured data. The ship speed is under-predicted by approximately 1.3% on the coarse and medium grids, while the fine grid solution is within 0.1% compared to the data from the measured mile test. Hence, convergence with grid refinement is not achieved for the final ship speed. Following Simonsen et al. (2013), the grid uncertainty is evaluated as a maximum deviation between the three results:



(a) Convergence of the forward speed,

$$U_V = F_S(V_{\max} - V_{\min}), \quad (25)$$

where $F_S = 3$ is the safety factor (Stern et al., 2001). The resulting grid uncertainty for the achieved speed is 4.02%, or 0.85 knots. The achieved propeller rotation rate is 126.27 RPM, with a relative error of 0.24% compared to the measured mile data, with the corresponding grid uncertainty of 2.20% or 2.78 RPM.

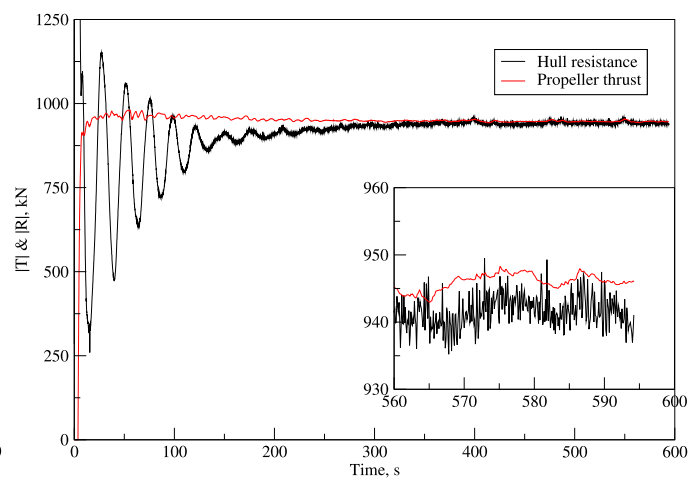
Fig. 8(b) presents the convergence of forces during the CFD simulation with the fine grid. During the last 250 s of the simulation, the resistance oscillates within $\pm 1\%$. Note that for the REGAL ship, the force oscillations are twice as high ($\pm 2.5\%$) because of the breaking bow wave, see Fig. 6(a). The waves at the bow of the Uljanik car carrier are mild and low in amplitude due to bulbous bow, as seen in Fig. 9(a). The wave field at the stern and the dynamic pressure at the propeller plane are presented in Fig. 9(b).

It is also important to note that the average value of resistance and the propeller thrust are not perfectly balanced throughout last 50 s, indicating the need to run the simulation longer. This is a direct consequence of the PI controller (see (24)) that has been used for these simulations. Better convergence properties may be obtained by tuning the PI controller and implementing different variants of controllers, which is out of scope of this work. Note that the thrust is on average approximately 0.3% higher, which is deemed negligible as the forward speed of the ship does not vary significantly as seen in Fig. 8(a).

CPU times required to perform self-propulsion simulations for the car carrier are presented in Table 4. Since the grids are smaller compared to the first test case, 16 to 32 cores have been used in order to achieve the final solution within 6 h and 16 h.

4. Conclusion and future work

A direct comparison of full scale CFD self-propulsion simulations with sea trials is presented for two ships: a general cargo carrier and a car carrier. The actuator disc model is used for the propeller along with the existing two-phase, incompressible and turbulent CFD algorithm in the Naval Hydro pack, which is based on foam-extend, a fork of the OpenFOAM software. Both ships were in ballast condition, where a fixed propeller rotation rate has been prescribed for the general cargo carrier and a target 80%MCR has been prescribed for the car carrier. The target 80%MCR is achieved by employing a PI controller.



(b) Convergence of forces.

Fig. 8. CFD results for Uljanik car carrier.

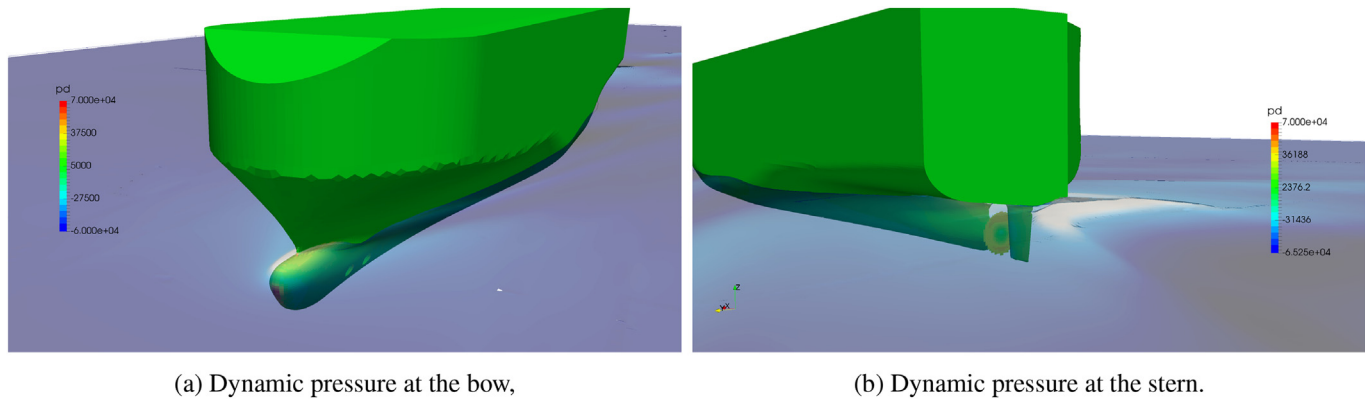


Fig. 9. Dynamic pressure field in bow and stern regions for Uljanik car carrier.

Table 4
CPU times for car carrier self-propulsion simulations.

Grid	Coarse	Medium	Fine
Number of cells	1 673 545	2554 135	6 405 264
Number of cores	16	32	32
CPU time per time-step, s	6.4	5.3	14.3
CPU time per second of real time	64.3	53.0	142.6
CPU time until convergence, h	10.7	5.9	15.8

The achieved speed predicted with CFD compares very well to sea trial measurements, where the relative error is within 0.3% for both ships. For the general cargo carrier, trim angle is under-predicted compared to sea trials by approximately 0.02° . The relative error of achieved propeller rotation rate for the car carrier is approximately 0.24%. By performing grid sensitivity studies, we estimated the grid uncertainty for the achieved forward speed to be reasonably low: approximately 0.15% for the general cargo carrier and 4.02% for the car carrier. Lower numerical uncertainty for the general cargo carrier is obtained since we have achieved oscillatory convergence, compared to the car carrier where we have not achieved convergence with grid refinement, thus using a higher safety factor equal to 3. However, it is important to note that this is not a strict verification study since the refinement ratios between grids are too low and not uniform. A strict verification study will be the topic of future work due to limited computational resources at present time. Still, the grid sensitivity study and the simplified uncertainty assessment allowed us to quantify a spread in the results when using different grids. As seen from the reported CPU times for particular cases, a very good solution compared to sea trial can be obtained in a single to few days.

The preliminary validation and grid sensitivity study for full scale ship hydrodynamics presented in this work is encouraging, although a lot of scientific and industrial effort must be invested in systematically quantifying numerous uncertainties that inevitably arise when directly comparing CFD results with sea trials, such as: propeller modelling, weather conditions, turbulence modelling, wall roughness modelling, elasticity of the ship (hogging/sagging), inertial properties of the ship, etc.

Acknowledgements

This research was sponsored by Bureau Veritas and Hyundai Heavy Industries under the administration of Dr. Šime Malenica and Dr. Geon-Hong Kim, whose support is gratefully acknowledged. The authors extend their sincere gratitude towards Lloyd's Register for organising and hosting the Workshop on Ship Scale Computer

Simulations (Lloyd's Register, 2016; Ponkratov, 2017), namely Dr. Dmitry Ponkratov who was in charge of the project. Our sincerest gratitude also goes to Uljanik's design office who agreed to share their valuable sea trial data with us, namely Mr. Vito Radolović, Mr. Josip Andrišić, Mr. Obrad Kuzmanović and Mr. Igor Lalović. Without their support, it would be close to impossible to perform this study comparing the CFD results directly to sea trial measurements. The authors thank their reviewers since the article has significantly benefited from their valuable comments.

References

- Aulisa, E., Manservigi, S., Scardovelli, R., Zaleski, S., 2003. A geometrical area-preserving Volume-of-Fluid advection method. *J. Comput. Phys.* 192 (1) <https://doi.org/10.1016/j.jcp.2003.07.003>.
- Batchelor, F.R., 1967. *An Introduction to Fluid Dynamics*. Cambridge University Press.
- Beaudoin, M., Jasak, H., 2008. Development of generalized grid interface for turbomachinery simulations with OpenFOAM. In: *Proceedings of the Open Source CFD International Conference*.
- Carrica, P., Castro, A., Stern, F., 2010. Self-propulsion computations using a speed controller and a discretized propeller with dynamic overset grids. *J. Mar. Sci. Technol.* 15, 316–330. <https://doi.org/10.1007/s00773-010-0098-6>.
- Carrica, P.M., Fu, H., Stern, F., 2011. Computations of self-propulsion free to sink and trim and of motions in head waves of the KRISO Container Ship (KCS) model. *Appl. Ocean Res.* 33, 309–320.
- Carrica, P.M., Mofidi, A., Martin, E., 2015. Progress toward Direct CFD simulation of Manoeuvres in waves. In: *Proceedings of the MARINE 2015 Conference*, pp. 327–338.
- Castro, A., Carrica, P.M., Stern, F., 2011. Full scale self-propulsion computations using discretized propeller for the KRISO container ship KCS. *Comput. Fluids* 51, 35–47. <https://doi.org/10.1016/j.compfluid.2011.07.005>.
- Demirdžić, I., 2015. On the discretization of the diffusion term in finite-volume continuum mechanics. *Numer. Heat Transf. Part B* 68, 1–10. <https://doi.org/10.1080/10407790.2014.985992>.
- Desjardins, O., Moureau, V., Pitsch, H., 2008. An accurate conservative level set/ghost fluid method for simulating turbulent atomization. *J. Comput. Phys.* 227 (18), 8395–8416.
- Eca, L., Hoekstra, M., 2014. A procedure for the estimation of the numerical uncertainty of CFD calculations based on grid refinement studies. *J. Comput. Phys.* 262, 104–130. <https://doi.org/10.1016/j.jcp.2014.01.006>.
- Ferziger, J.H., Peric, M., 1996. *Computational Methods for Fluid Dynamics*. Springer.
- Huang, J., Carrica, P.M., Stern, F., 2007. Coupled ghost fluid/two-phase level set method for curvilinear body-fitted grids. *Int. J. Numer. Meth. Fluids* 44, 867–897. <https://doi.org/10.1002/flid.1499>.
- Issa, R.I., 1986. Solution of the implicitly discretised fluid flow equations by operator-splitting. *J. Comput. Phys.* 62, 40–65.
- Jacobsen, N.G., Fuhrman, D.R., Fredsøe, J., 2012. A wave generation toolbox for the open-source CFD library: OpenFoam®. *Int. J. Numer. Meth. Fluids* 70 (9), 1073–1088. <https://doi.org/10.1002/flid.2726>.
- Jasak, H., 1996. *Error Analysis and Estimation for the Finite Volume Method with Applications to Fluid Flows*. Ph.D. thesis. Imperial College of Science, Technology & Medicine, London.
- Jasak, H., Weller, H., Gosman, A., 1999. High resolution NVD differencing scheme for arbitrarily unstructured meshes. *Int. J. Numer. Meth. Fluids* 31, 431–449.
- Jasak, H., Vukčević, V., Gatin, I., 2015. Numerical simulation of wave loads on static offshore structures. In: *CFD for Wind and Tidal Offshore Turbines*. Springer Tracts in Mechanical Engineering, pp. 95–105.

- Juretić, F., 2017. cfMesh: Advanced Meshing Tool. cfMesh.com [Online; Accessed 22 February 2017].
- Kim, G.-H., Jun, J.-H., 2015. Numerical simulations for predicting resistance and self-propulsion performances of JBC using OpenFOAM and star-CCM+. In: Proceedings of the Tokyo 2015: a Workshop on CFD in Ship Hydrodynamics, vol. 3, pp. 285–296.
- Krasilnikov, V., 2013. Self-propulsion RANS computations with a single-screw container ship. In: Proceedings of the Third International Symposium on Marine Propulsors, pp. 430–438.
- Lalanne, B., Villegas, L.R., Tanguy, S., Risso, F., 2015. On the computation of viscous terms for incompressible two-phase flows with level set/ghost fluid method. *J. Comput. Phys.* 301, 289–307.
- Larsson, L., Stern, F., Visonneau, M., Hirata, N., Hino, T., Kim, J. (Eds.), 2015. Tokyo 2015: a Workshop on CFD in Ship Hydrodynamics, vol. 2. NMRI (National Maritime Research Institute), Tokyo, Japan.
- Larsson, L., Stern, F., Visonneau, M., Hirata, N., Hino, T., Kim, J. (Eds.), 2015. Tokyo 2015: a Workshop on CFD in Ship Hydrodynamics, vol. 3. NMRI (National Maritime Research Institute), Tokyo, Japan.
- Lloyd's Register, 2016. A Workshop on Ship Scale Hydrodynamic Computer Simulation. <http://www.lr.org/en/news-and-insight/events/ship-scale-hydrodynamics-numerical-methods-workshop.aspx> [Online; Accessed 22 February 2017].
- Menter, F.R., Kuntz, M., Langtry, R., 2003. Ten years of industrial experience with the SST turbulence model. *Turb. Heat Mass Transf.* 4, 625–632.
- Patankar, S.V., Spalding, D.B., 1972. A calculation procedure for heat, mass and momentum transfer in three-dimensional parabolic flows. *Int. J. Heat Mass Transf.* 15, 1787–1806.
- Ponkratov, D. (Ed.), 2017. Proceedings: 2016 Workshop on Ship Scale Hydrodynamic Computer Simulations. Lloyd's Register, Southampton, United Kingdom.
- Ponkratov, D., Zegos, C., 2014. Ship scale CFD self-propulsion simulation and its direct comparison with sea trial results. In: Proceedings of the International Conference on Computational and Experimental Marine Hydrodynamics (MARHY'14).
- Ponkratov, D., Zegos, C., 2015. Validation of ship scale CFD self-propulsion simulation by the direct comparison with sea trial results. In: Proceedings of the Fourth International Symposium on Marine Propulsors.
- Queutey, P., Visonneau, M., 2007. An interface capturing method for free-surface hydrodynamic flows. *Comput. Fluids* 36, 1481–1510. <https://doi.org/10.1002/j.compfluid.2006.11.007>.
- R. MPEC.245(66), 2014. Guidelines on the Method of Calculation of the Attained EEDI for New Ships, Adopted on 2 March 2012.
- Røenby, J., Bredmose, H., Jasak, H., 2016. A computational method for sharp interface advection. *Open Sci.* 3 (11) <https://doi.org/10.1098/rsos.160405>.
- Rusche, H., 2002. Computational Fluid Dynamics of Dispersed Two - Phase Flows at High Phase Fractions. Ph.D. thesis. Imperial College of Science, Technology & Medicine, London.
- Šeb, B., 2017. Numerical Characterisation of a Ship Propeller. Master's thesis. Faculty of Mechanical Engineering and Naval Architecture, University of Zagreb.
- Shen, Z., Wan, D., Carrica, P.M., 2015. Dynamic overset grids in OpenFOAM with application to KCS self-propulsion and maneuvering. *Ocean Eng.* 108, 287–306. <https://doi.org/10.1016/j.oceaneng.2015.07.035>.
- Simonsen, C.D., Otzen, J.F., Joncquey, S., Stern, F., 2013. EFD and CFD for KCS heaving and pitching in regular head waves. *J. Mar. Sci. Technol.* 18, 435–459. <https://doi.org/10.1007/s00773-013-0219-0>.
- Stern, F., Wilson, R.V., Coleman, H.W., Paterson, E.G., 2001. Comprehensive approach to verification and validation of CFD Simulations—Part 1: methodology and procedures. *J. Fluid Eng.* 123 (4), 793–802. <https://doi.org/10.1115/1.1412235>.
- Tzabiras, G., Polyzos, S., Zarafonitis, G., 2009. Self-propulsion simulations of passenger—Ferry ships with bow and stern propulsors. In: Proceedings of the 12th Numerical Towing Tank Symposium (NUTTS).
- Ubbink, O., Issa, R.I., 1999. A method for capturing sharp fluid interfaces on arbitrary meshes. *J. Comput. Phys.* 153, 26–50.
- van Leer, B., 1977. Towards the ultimate conservative difference scheme. IV. A new approach to numerical convection. *J. Comput. Phys.* 23, 276–299.
- Visonneau, M., Deng, G., Guilmineau, E., Queutey, P., Wackers, J., 2016. Local and global assessment of the flow around the Japan bulk carrier with and without energy saving devices at model and full scale. In: Proceedings of the 31st Symposium on Naval Hydrodynamics.
- Vukčević, V., 2016. Numerical Modelling of Coupled Potential and Viscous Flow for Marine Applications - in Preparation. Ph.D. thesis. Faculty of Mechanical Engineering and Naval Architecture, University of Zagreb. <https://doi.org/10.13140/RG.2.2.23080.57605>.
- Vukčević, V., Jasak, H., Gatin, I., 2017. Implementation of the ghost fluid method for free surface flows in polyhedral finite volume framework. *Comput. Fluids* 153, 1–19. <https://doi.org/10.1016/j.compfluid.2017.05.003>.
- Weller, H.G., Tabor, G., Jasak, H., Fureby, C., 1998. A tensorial approach to computational continuum mechanics using object oriented techniques. *Comput. Phys.* 12, 620–631.
- Xing-Kaeding, Y., Gatchell, S., 2015. Resistance and self-propulsion predictions for Japan bulk carrier without and with duct using the FreSCO+ code. In: Proceedings of the Tokyo 2015: a Workshop on CFD in Ship Hydrodynamics, vol. 3, pp. 291–296.